Interfacial Self-Assembly Driven Formation of Hierarchically Structured Nanocrystals with Photocatalytic Activity

Yong Zhong,[†] Zixuan Wang,[†] Ruifang Zhang,[†] Feng Bai,[†,‡,*] Huimeng Wu,[§] Raid Haddad,[‡] and Hongyou Fan[‡,§,*]

[†]Key Laboratory for Special Functional Materials of the Ministry of Education, Henan University, Kaifeng 475004, P. R. China, [‡]The University of New Mexico/NSF Center for Micro-Engineered Materials, Department of Chemical and Nuclear Engineering, Albuquerque, New Mexico 87131, United States, and [§]Sandia National Laboratories, Advanced Materials Laboratory, Albuquerque, New Mexico 87106, United States

ABSTRACT We report the synthesis of hierarchical structured nanocrystals through an interfacial self-assembly driven microemulsion (μ-emulsion) process. An optically active macrocyclic building block Sn (IV) *meso*-tetraphenylporphine dichloride (tin porphyrin) is used to initiate noncovalent self-assembly confined within μ-emulsion droplets. *In-situ* studies of dynamic light scattering, UV–vis spectroscopy, and electron microscopy, as well as optical imaging of reaction processes suggest an evaporation-induced nucleation and growth self-assembly mechanism. The resulted nanocrystals exhibit uniform shapes and sizes from ten to a hundred nanometers. Because of the spatial ordering of tin porphyrin, the hierarchical nanocrystals exhibit collective optical properties resulting from the coupling of molecular tin porphyrin and photocatalytic activities in the reduction of platinum nanoparticles and networks and in photodegradation of methyl orange (MO) pollutants.

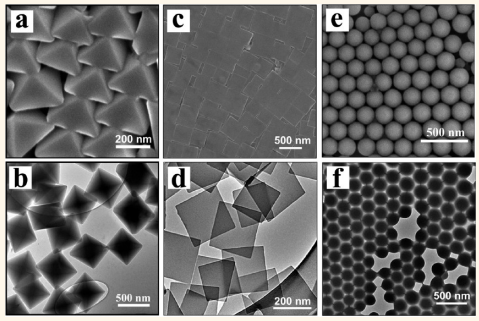

KEYWORDS: self-assembly · nanocrystals · photocatalytic · nanoparticles · emulsion

Molecular self-assembly is a powerful method to synthesize nanostructured materials.[1−11] The unique property of molecular assemblies has been shown to depend not only on the size, shape, and composition of the molecular building blocks but also to a large extent on ordered spatial arrangement within an assembly.[6−13] Despite recent advances in the assembly of molecule building blocks and formation of well-defined superstructures,[14−20] the synthesis of hierarchical structures leveraging the structural advantages of individual molecules still remains a significant challenge. The development of more facile and efficient methods for rationally designing and fabricating molecular assemblies is critically important for the continued advancement of this area. While previous efforts have focused on controlled 2D and 3D fabrication over a limited range of scales, developments of new molecular and building block designs and strategies of functionalization are essential for directing structure and property control over multiple scales.[21−23]

We previously developed the interfacially driven microemulsion (μ-emulsion) method to initiate self-assembly and formation of hierarchically structured nanoparticle arrays.[24−26] In our previous work, μ-emulsions were fabricated through dispersion of an organic solution containing nanoparticles as the building block to another immiscible aqueous solution; subsequently, we removed organic solvent through thermally driven evaporation, which induces nanoparticles self-assembly that was confined within μ-emulsion droplets. The balanced interactions (e.g., van der Waals, dipole–dipole interactions, particle–particle attractions, *etc.*) between nanoparticles lead to formation of ordered nanostructured particle arrays. Herein, we extended this method to synthesize hierarchically structured active nanocrystals by using an optically active macrocyclic molecule, tin(IV) *meso*-tetraphenylporphine dichloride (tin porphyrin, see Supporting Information Figure S1) as a building block. The emulsion was formed through mixing tin porphyrin chloroform

* Address correspondence to baifengsun@gmail.com, hfan@sandia.gov.

Received for review October 21, 2013 and accepted December 18, 2013.

Published online December 18, 2013
10.1021/nn405492d

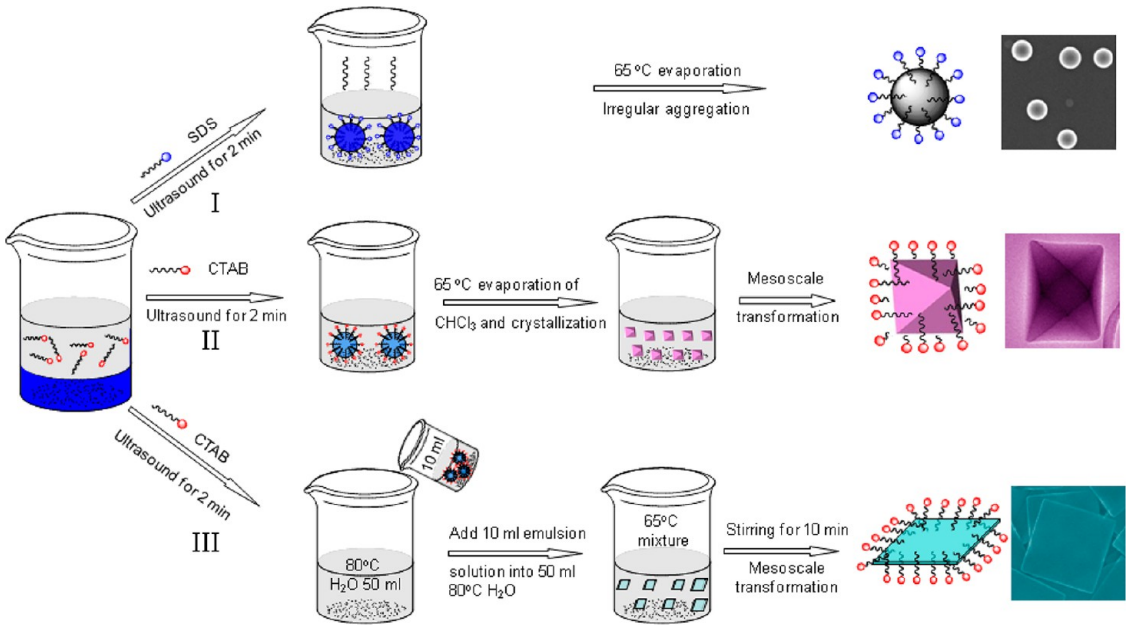

Figure 1. Schematic illustration of the synthesis processes of porphyrin nanocrystals by the μ-emulsion method.

solution with an aqueous solution containing surfactants. The oil-to-water volume ratio was controlled to be 1:10 (see Materials and Methods for detailed experimental procedures). By means of vigorous stirring (greater than 1500 rpm) or sonication, we obtained a surfactant-stabilized oil-in-water μ-emulsion in which tin porphyrin molecules were well dispersed inside μ-emulsion droplets. The low-boiling solvent (e.g., $CHCl_3$) was subsequently evaporated from the μ-emulsion system by heating to a given temperature. As solvent evaporates from the μ-emulsion droplets, the droplets shrink and the porphyrin concentration therein rises, inducing self-assembly of porphyrin molecules through noncovalent interactions inside the confined 3D oil-emulsion droplet spaces. Through noncovalent interactions such as $\pi-\pi$ stacking, ligand coordination, *etc.*, porphyrins self-assemble into ordered nanostructures.[1,19,21,22] Depending on the reaction conditions (see Figure 1), various hierarchically structured nanocrystals such as nanosheets, octahedra, and microspheres were obtained. The final products were collected and purified by centrifugation, then redispersed in DI-water.

RESULTS AND DISCUSSION

The tin porphyrin nanocrystals exhibit different morphologies depending on reaction conditions. Figure 2 shows electron microscopy (EM) images of these nanostructures. When we used cetyltrimethyl ammonium bromide (CTAB) surfactant, octahedra were obtained, as shown in the electron microscopy images (Figure 2a,b). The images show that the octahedra have good uniformity, well-defined facets, and sharp edges and corners. The average edge length of an octahedron is measured to be 350 $\pm$ 30 nm, Supporting Information, Figure S2a shows a relatively narrow size distribution of the octahedra. The nanosheets are

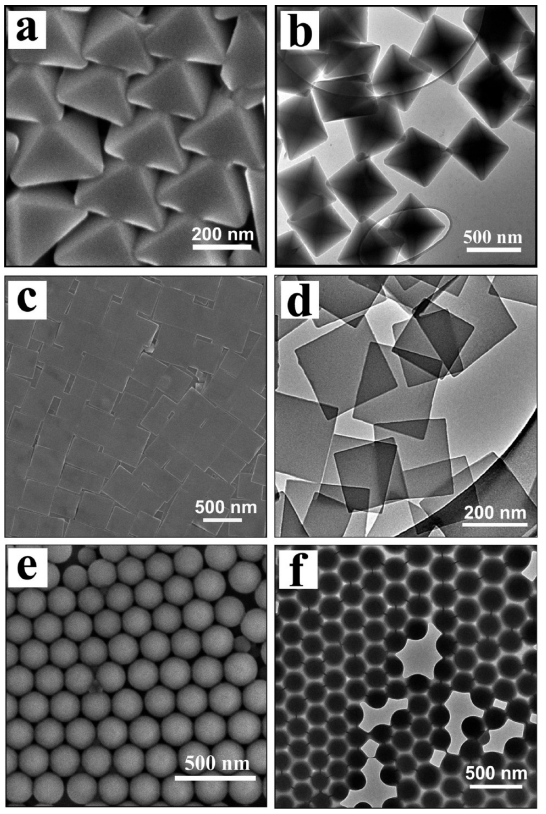

Figure 2. Structure and morphology of the hierarchically structured tin porphyrin nanocrystals: (a) representative SEM image of the self-assembled octahedral arrays; (b) TEM image of the octahedra; (c) SEM image of the self-assembled nanosheets; (d) TEM image of the individual nanosheets; (e) SEM image of the self-assembled microspheres, and (f) TEM image of individual microspheres.

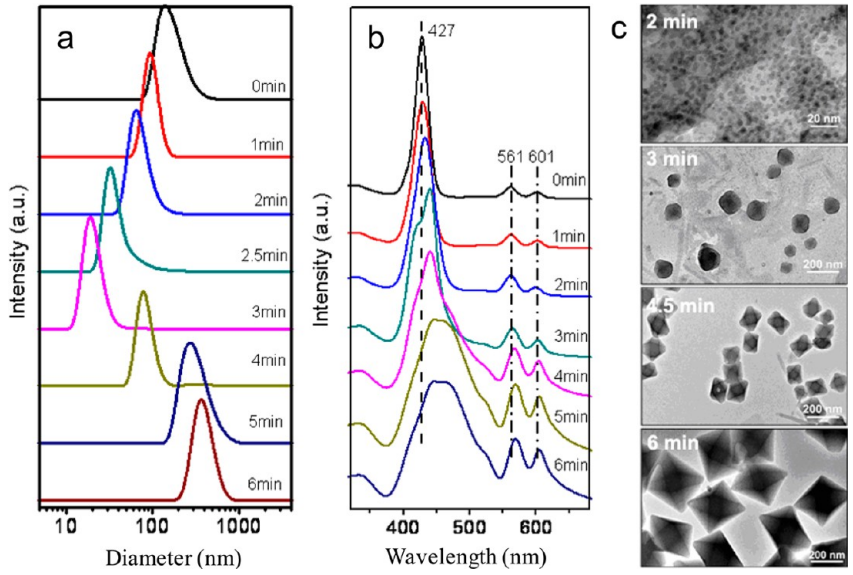

Figure 3. Time-course studies of the growth of tin porphyrin octahedral nanocrystals: (a) size evolution of emulsion droplets and nanocrystals in the emulsion solution at different reaction times measured by DLS; (b) UV−vis spectra of the emulsion solution at different times; (c) TEM images of the nanocrystals collected at different reaction times.

square in shape with edge length ranging from 300 to 500 nm as shown in Figure S2b. The nanosheets are very thin as shown the crossing section scanning electron microscopy (SEM) image in Figure S3. Transmission electron microscopy (TEM) images (Figure 2b,d) exhibit no defects in electron contrast within each octahedron and nanosheet. The average diameter of microspheres was measured to be 210 ± 10 nm (see Figure S2c in Supporting Information,). Owing to the monodisperse nature, these nanocrystals can self-assemble into ordered arrays on the silicon wafer or the TEM grid, which indicates that the tin porphyrin nanocrystals may serve as mesoscale building units for more complex macroscopic functional architectures.

Powder X-ray diffraction (XRD) patterns were collected for these nanocrystals. For tin porphyrin octahedra, XRD data show crystal patterns with major peaks between 5° and 30° (see Figure S4 in Supporting Information). The XRD patterns can be indexed as tetragonal space group *I4/m* (number 87) with unit cell dimensions $a = b = 13.673$ Å, $c = 9.961$ Å, $\alpha = \beta = \gamma = 90°$. Figure S4b and Figure S4c show the crystal structures solved from the XRD data. In this crystal structure, the porphyrin macrocycles lie flat in the $a-b$ plane with core Sn atoms at the corners and centers of the unit cells. As such, each molecule has 12 neighbors with which it interacts; 8 neighbors offset above and below its plane (stronger interactions), and 4 neighbors in-plane (weaker interactions). Periodic semiempirical calculations (PM6) find the crystal's binding energy to be 72 kJ/mol. For the nanosheets, XRD data exhibit fewer peaks than that of the octahedra. The weak XRD pattern is probably due to the very low thickness of the nanosheets. In addition, the 2D nanosheets lie flat on the substrate. This leads to an orientated crystal structure that yields few XRD patterns. No peaks are found in XRD data for the tin porphyrin microspheres, suggesting that they are amorphous.

The growth process of the octahedral nanocrystals was monitored *in situ* using dynamic light scattering (DLS), UV−vis spectroscopy, and TEM, as well as optical imaging. The results overall suggest an evaporation-induced nucleation and growth self-assembly mechanism. At the beginning of the self-assembly processes, when oil and water phases were mixed together, μ-emulsion droplets were rapidly formed which were measured by DLS to have average diameter of ~130 nm (Figure 3a). As the reaction progresses under the heat treatment, DLS data show that the μ-emulsion droplets gradually shrink to ~20 nm by 3 min. This shrinkage is due to the evaporation of the organic solvent with heating. TEM images (Figure 3c) indicate that in the first 3 min, small nanoparticle nuclei are formed. After 3 min, DLS results indicate that the nuclei starts to grow to 70 nm at 4 min, 250 nm at 5 min, and ~350 nm at 6 min. TEM images show that at 4.5 min, the nanoparticles are ~150 nm and the octahedral shape is clearly observed in some nanoparticles. UV−vis spectra further confirm that the self-assembly occurs *via* noncovalent packing (Figure 3b). At 0 min, the spectrum shows a major peak at 427 nm that belongs to lone tin porphyrin molecules. Along the time course of the organic solvent evaporation, the major peak starts to red shift and split with a shoulder peak. This spectral shifting and splitting is consistent with previous observations for j-aggregation through noncovalent interactions. After 3 min, the Soret band becomes much broader and the Q-band also shifts to red, both indicative of extensive noncovalent bonding or interactions. The resulting color changes of the

emulsion solution at different evaporation times were monitored. The crystallization process is nicely observed by the change of the μ-emulsion color from violet (0 min) to transparent light brown (3 min) to dark brown (6 min). At the beginning of the self-assembly process, the solution exhibits milky and purple color. Formation of μ-emulsion causes the solution to be milky and not transparent. The purple color is from the molecular tin porphyrin. After 3 min, small nanocrystals started to form, which makes the solution to be light brown. Because the initial nanocrystals are small (<20 nm), the solution is still transparent. Along the growth of the nanocrystals, they become bigger and bigger and start to scatter visible light. Finally the solution turns dark brown.

During the synthesis of tin porphyrin octahedra, we used CTAB surfactants to form μ-emulsions that initiate the self-assembly processes. However, when we replaced CTAB with sodium dodecyl sulfate (SDS), we found out that tin porphyrin microspheres were formed instead of octahedra. At the beginning of the self-assembly process, μ-emulsion droplets with a diameter of ~500 nm were formed. DLS data show that along with the time course of heating, the μ-emulsion droplets start to shrink from 500 nm to ~160 nm until 4 min (Supporting Information, Figure S5a). The particles sizes remain around 160 nm after that. No nucleation of tin porphyrin is observed during this progress. UV−vis spectra further supported this observation. UV−vis spectra showed only a major peak at 427 nm that attributes to tin porphyrin molecules, which suggests that tin porphyrin self-assembly did not occur. Instead, the tin porphyrin molecules just irregularly aggregate within the microspheres. This was confirmed by XRD patterns that show no crystalline peaks (Supporting Information, Figure S4). The different nanocrystal morphologies might be due to the nature of interactions of surfactants with tin porphyrins. In the case of SDS, the anionic head groups SO_4^{2-} of SDS might bind with Sn in the porphyrin molecule, which prohibits the nuclei and mesoscale reorientation of tin porphyrin.[27,28] Our X-ray photoelectron spectroscopy (XPS) results (Supporting Information, Figure S6) confirmed the interactions between the headgroup of SDS and tin porphyrins. This interaction again prohibits tin porphyrin self-assembly through noncovalent interactions. The evaporation of organic solvents resulted in amorphous microspheres instead of crystalline octahedra. In the case of CTAB, we did not observe such interactions between surfactant head groups and tin porphyrins from XPS studies. Thus, CTAB played the sole role of a surfactant to form emulsion and confined noncovalent self-assembly of tin porphyrin into crystalline octahedra. To further testify this mechanism, we used similar surfactants such as anionic surfactant sodium dodecyl benzene sulfonate (SDBS) and cation surfactant myristyltrimethyl ammonium bromide (MTAB) to repeat the self-assembly processes. Results were very consistent with our above explanation. SEM images reveal that tin porphyrin formed octahedra in the MTAB case and microspheres in the SDBS case as shown (see Figure S7 in Supporting Information).

It was found that a change of evaporation temperature has a great impact on the formation of nanosheets. A μ-emulsion solution (same as the reaction solution used for synthesis of tin porphyrin octahedra) was heated at different temperature for the synthesis of tin porphyrin nanocrystals. We found that the relative amount of the octahedra to the nanosheets decreases with an increase of temperature, as shown in Supporting Information, Figure S8. This might be due to the formation of the CTAB lamellar mesophase, which confines formation of nanosheets morphology. A detailed formation mechanism of nanosheets is still under investigation.

We found that the size of the tin porphyrin self-assembled octahedra can be easily tuned by varying the surfactant concentration. As shown in Supporting Information, Figure S9, the tin porphyrin octahedra diameters increased from 85 to 440 nm dramatically while their polydisperse index (PDI) remained narrow, with the CTAB concentration increasing from 0.004 to 0.025 M. Similar phenomena were observed in the previous works for the synthesis of molecular-based materials in bottom-up fashion using surfactant-assisted self-assembly.[29,30] The B-band becomes much broader and the Q-band also shifts to red with the octahedral diameter increasing, and there was a shoulder peak around 500 nm. These results indicate that tin porphyrin units were packed more orderly in longer-distances in bigger samples.

The final octahedra and nanosheets exhibit absorption and emission spectra that are more complicated than those of the precursors. These new optical signatures are likely due to the coupling arising from the well-ordered spatial packing of the tin porphyrins. While the UV−vis spectrum of tin porphyrin in $CHCl_3$ shows a Soret band at 426 nm and Q-bands at 562 and 600 nm, those of the octahedrons, nanosheets, and spheres are more complex (Figure 4).

Drawing inspiration from the photocatalytic role that assemblies of porphyrin molecules play in nature,[31,32] we utilized these nanostructures for the templated synthesis of metals nanoparticles and networks *via* photocatalytic reduction of a metal−salt precursor.[33] In a typical procedure for the synthesis of Pt nanoparticles and networks (see details in Materials and Methods), K_2PtCl_4 stock solution 0.5 mL (10 mM) and ascorbic acid stock solution 0.5 mL (0.1 M) were added to a 20 mL glass vial containing 10 mL of the ZnTPyP nanostructures with a concentration of 0.1 mg/mL. The reaction mixture was sonicated to homogenize the solution and then irradiated with incandescent light (800 nmol cm^{-2} s^{-1}) for 30 min.

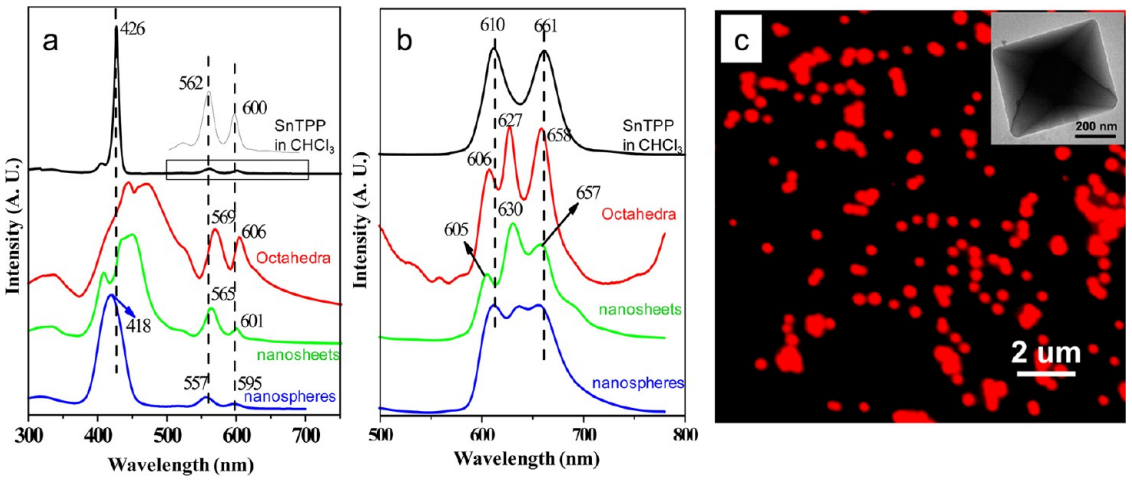

Figure 4. Optical characterization of hierarchically structured tin porphyrin nanocrystals: (a) UV−vis and (b) fluorescence spectra of different tin porphyrin nanocrystals as well as tin porphyrin molecules in $CHCl_3$. (c) Fluorescence image of tin porphyrin octahedra.

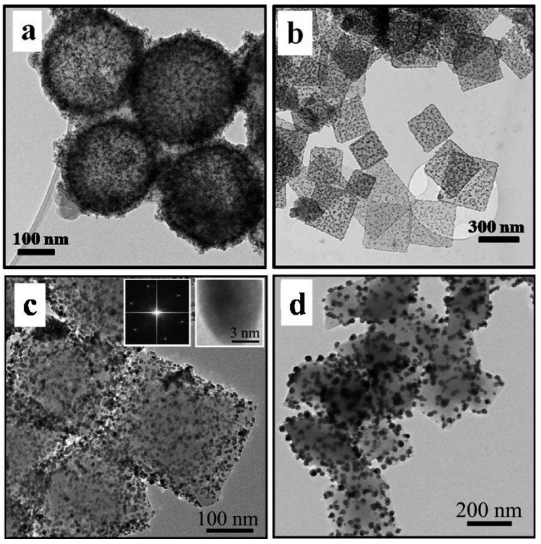

Figure 5. Electron microscopy images of the metal nanocrystals grown on tin porphyrin nanostructures. TEM images of (a) Pt/tin porphyrin nanosphere composites; (b) Pt/tin porphyrin nanosheet composites; (c) Pd/tin porphyrin octahedra composites composites; (d) Ag/tin porphyrin octahedra composites.

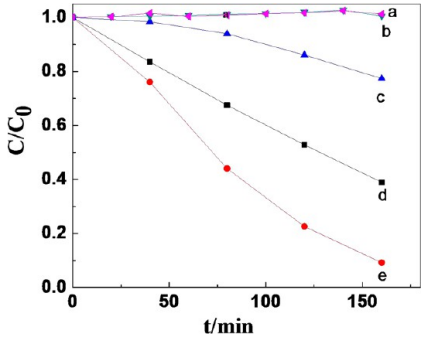

Figure 6. Photocatalytic activities of tin porphyrin nanospheres (e), octahedra (d), and nanosheets (c) for photo degradation of MO molecules under visible light irradiation. The results from blank experiments, where no tin porphyrin nanocrystals were used (a) and where commercial P25 (b) was used are also presented for comparison.

The reaction solution initially appears purple in color under incandescent light due to light scattering by the porphyrin nanocrystals. As the photocatalytic reaction proceeds, the reaction solution turns black, suggesting that Pt^0 is formed. Through centrifugation, we collect the final black nanostructured Pt/porphyrin composite materials. Figure 5 shows the TEM results of the photocatalytic reduction of Pt using tin porphyrin nanosheets (a) and nanospheres (b) as templates, and Pd (c), Ag (d) using tin porphyrin octahedra as templates. At a relatively low concentration of K_2PtCl_4, single Pt nanoparticles are formed, ~3.2 nm in size. On increasing K_2PtCl_4 concentration to 0.2 mM, the Pt nanoparticles start to interconnect with each other and form a 3D network (Figure 5A). Both TEM and XRD data (Figure S10 in Supporting Information) confirm the formation of Pt single crystals.

The catalytic activity for photodegradation of Methyl Orange (MO) pollutant was also investigated under visible light irradiation. Figure 6 shows the photocatalytic activities of different tin porphyrin nanocrystals. We found several interesting features: first, all tin porphyrin nanocrystals show photocatalytic activity for photodegrading of MO; second, all tin porphyrin nanocrystals show better catalytic activity than commercial P25 catalysts; finally, the tin porphyrin nanocrystals show an interesting morphology-dependent photocatalytic activity. When the tin porphyrin nanosheets were used in the system, only about 20% MO was degraded after 160 min. The photodegradation efficiencies of MO can reach above 60% and 90%, respectively, when tin porphyrin octahedra and nanospheres were used.

CONCLUSIONS

The interfacially driven microemulsion (μ-emulsion) process is a facile method to synthesize monodisperse

tin porphyrin nanocrystals with capability to control size and morphology. The hierarchical nanocrystals exhibit collective optical properties resulting from molecular tin porphyrin and photocatalytic reduction of platinum nanoparticles and networks and photodegrading of MO. This μ-emulsion method should be extendable to a wide variety of other building blocks such as C60, carbon nanotubes to form hierarchical nanostructures. The ease of formation of such well-defined nanocrystals should be favorable for investigation of their collective chemical and physical properties.

MATERIALS AND METHODS

Materials. Sn(IV) *meso*-tetraphenylporphine dichloride (tin porphyrin) was purchased from Frontier Scientific, Inc., cetyltrimethylammonium bromide (CTAB), myristyltrimethylammonium bromide (MTAB), sodium dodecyl benzene sulfonate (SDBS) and sodium dodecyl sulfate (SDS) were purchased from Aldrich Chemical Co. and used without further purification. NaOH (1 M) standard solution was purchased from Alfa Aesar and used without further purification. $AgNO_3$ (GR grade) was purchased from the Aladdin Reagent Company. Sodium thiosulfate ($Na_2S_2O_3$, AR), methyl orange (MO, AR), and all other chemicals were used without further purification. Silver(I) thiosulfate solution was freshly prepared before use according to a published procedure.[34] Palladium(II) chloride ($PdCl_2$, A.R.) was purchased from Shanghai Fine Chemicals Co., Ltd. Inc. A 10 mM Na_2PdCl_4 aqueous solution was freshly prepared by adding $PdCl_2$ in diluted hydrochloric acid solution to form H_2PdCl_4 aqueous solution, followed by dropwise addition of 1 N NaOH solution to adjust the pH to about 6. The solution was filtered through a 0.2 μm membrane prior to use. All the solutions were prepared in ultrapure water from a Barnstead Nanopure water system, and filtered through a 0.2 μm syringe filter to remove particles.

Materials Preparation. In a general preparation, 1 mL of tin porphyrin (10 mg/mL in chloroform) was added to 9 mL of aqueous solution of surfactants (CTAB or SDS 0.01M). This solution was then emulsified by ultrasonic treatment under gentle stirring for 2 min. The emulsion was subsequently heated in a water bath at 65 °C for about 10 min to evaporate $CHCl_3$. The resulting solution was centrifuged at 9000 rpm and washed twice with Millipore water to remove the surfactant.

Nanosheets Preparation. The 10 mL emulsion was prepared by the same emulsion process mentioned above using CTAB surfactant. The emulsion was subsequently added into 60 mL of hot water (60 °C; 70 °C; 80 °C) under stirring. The nanosheets were collected by centrifuging and redispersed in deionized water.

Self-metallization of tin porphyrin nanocrystals: In a 20 mL glass vial, under stirring, chemicals were added in the following order: 8 mL of water, 1 mL of silver(I) thiosulfate solution (20 mM), 1 mL of ascorbic acid stock solution (0.1 M), 2 mg of tin porphyrin nanocrystals, forming a purple solution. The solution was then irradiated with incandescent light (15 mW cm^{-2}). The reaction solution initially appears to be pink in color under incandescent light due to light scattering by tin porphyrin nanocrystals. As the photocatalytic reaction proceeds, the mixture shows a color change to gray and then to black, suggesting that Ag^0 is formed. After 30 min of reaction, the Ag@tin porphyrin hybrid materials were collected by centrifugation and washed with water. For others metal@tin porphyrin nanomaterials synthesis, we just changed the rare metal precursors.

Photodegradation of MO: Photocatalytic activity of tin porphyrin materials under visible light was evaluated by the degradation of MO in aqueous solutions according to a published procedure.[35] A 1 mg sample of tin porphyrin nanocrystals was dispersed in a 40 mL aqueous solution of methyl orange (MO) dye (20 mg/L), and the mixture was stirred for 30 min to establish an adsorption/desorption equilibrium before irradiation in a pyrex beaker made of quartz. The light source for the photocatalytic experiment was a 300 W xenon arc lamp installed in a laboratory lamp housing system (PLS-SXE 300/300UV, Beijing Perfect light Technology Co., Ltd. China). Before entering the photocatalytic reactor, the light passed through a 10 cm water filter and a UV cutoff filter (>400 nm). During the photodegradation, aliquots (4 mL) were taken out from the reaction system at given time intervals and centrifuged to remove the tin porphyrin nanocrystals. The filtrates were analyzed by recording the absorbance at the maximum at 464 nm in the UV−visible spectrum of MO. The degradation efficiency at time t was determined from the value of C/C_0, where C_0 is the initial concentration before the MO is kept in the dark and C is the concentration of MO at a certain real-time t. For comparison, blank experiments without catalyst and with 10 mg P25, where no tin porphyrin nanocrystals were added, were carried out. Negligible degradation of MO molecules could be observed.

Characterization. The powders were redispersed in pure water and deposited onto silicon wafer substrates and copper grids for the characterization of scanning electron microscopy (SEM) and transmission electron microscopy (TEM), respectively. SEM images were taken using a Hitachi 5200 FEG microscope. TEM was performed on a JEOL 2010 with 200 kV acceleration voltage, equipped with a Gatan slow scan CCD camera. The X-ray diffraction (XRD) spectra were recorded on a Siemens D500 diffractometer using Ni-filtered Cu Kα radiation with λ 1.54 Å. The size distributions of the tin porphyrin nanoparticles were determined with a Zetasizer nanozs (Malvern). XPS analysis was performed with a Kratos Axis Ultra system using monochromatic AlKα X-rays (1486.6 eV) operated at 150 W and 15 kV at a background pressure of approximately 5.0×10^{-9} Torr. A survey spot size and 40 eV pass energy were used for the analysis. A charge neutralizer was used, and all the binding energies were calibrated with respect to the hydrocarbon C1s peak at 284.8 eV.

Conflict of Interest: The authors declare no competing financial interest.

Supporting Information Available: Schematic illustration of preparation process, size distribution results, XRD patterns, crystal structures, XPS results, and SEM and TEM images at different reaction conditions. This material is available free of charge *via* the Internet at http://pubs.acs.org.

Acknowledgment. This work was supported by the U.S. Department of Energy, Office of Basic Energy Sciences, Division of Materials Sciences and Engineering. F.B. acknowledged the support from the National Natural Science Foundation of China (No. 21171049 and No. 50828302), Program for Science & Technology Innovation Talents in Universities of Henan Province (No. 13HASTIT009), and Program for Changjiang Scholars and Innovative Research Team in University (No. PCS IRT1126). TEM studies were performed in the Department of Earth and Planetary Sciences at University of New Mexico and Henan University. We acknowledge the use of the SEM facility supported by the NSF EPSCOR and NNIN grants. We thank Dr. Binbin Hu for his valuable discussions and help on the XPS. Sandia National Laboratories is a multiprogram laboratory managed and operated by Sandia Corporation, a wholly owned subsidiary of Lockheed Martin Corporation, for the U.S. Department of Energy's National Nuclear Security Administration under Contract No. DE-AC04-94AL85000.

REFERENCES AND NOTES

1. Drain, C. M. Self-Organization of Self-Assembled Photonic Materials into Functional Devices: Photo-switched Conductors. *Proc. Natl. Acad. Sci. U.S.A.* **2002**, *99*, 5178–5182.

2. Du, C.; Falini, G.; Fermani, S.; Abbott, C.; Moradian-Oldak, J. Supramolecular Assembly of Amelogenin Nanospheres into Birefringent Microribbons. *Science* **2005**, *307*, 1450–1454.
3. Kurth, D. G.; Lehmann, P.; Schütte, M. A Route to Hierarchical Materials Based on Complexes of Metallosupramolecular Polyelectrolytes and Amphiphiles. *Proc. Natl. Acad. Sci. U.S.A.* **2000**, *97*, 5704–5707.
4. Park, S.; Lim, J.-H.; Chung, S.-W.; Mirkin, C. A. Self-Assembly of Mesoscopic Metal−Polymer Amphiphiles. *Science* **2004**, *303*, 348–351.
5. Winfree, E.; Liu, F.; Wenzler, L. A.; Seeman, N. C. Design and Self-Assembly of Two-Dimensional DNA Crystals. *Nature* **1998**, *394*, 539–544.
6. Jiang, L.; Fu, Y.; Li, H.; Hu, W. Single-Crystalline, Size, and Orientation Controllable Nanowires and Ultralong Microwires of Organic Semiconductor with Strong Photoswitching Property. *J. Am. Chem. Soc.* **2008**, *130*, 3937–3941.
7. Zhang, Y.; Chen, P.; Jiang, L.; Hu, W.; Liu, M. Controllable Fabrication of Supramolecular Nanocoils and Nanoribbons and Their Morphology-Dependent Photoswitching. *J. Am. Chem. Soc.* **2009**, *131*, 2756–2757.
8. Che, Y.; Datar, A.; Balakrishnan, K.; Zang, L. Ultralong Nanobelts Self-Assembled from an Asymmetric Perylene Tetracarboxylic Diimide. *J. Am. Chem. Soc.* **2007**, *129*, 7234–7235.
9. Han, W.; Byun, M.; Li, B.; Pang, X.; Lin, Z. A Simple Route to Hierarchically Assembled Micelles and Inorganic Nanoparticles. *Angew. Chem., Int. Ed.* **2012**, *51*, 12588–12592.
10. Byun, M.; Han, W.; Li, B.; Xin, X.; Lin, Z. An Unconventional Route to Hierarchically Ordered Block Copolymers on a Gradient Patterned Surface through Controlled Evaporative Self-Assembly. *Angew. Chem., Int. Ed.* **2013**, *52*, 1122–1127.
11. Han, W.; Lin, Z. Learning from "Coffee Rings": Ordered Structures Enabled by Controlled Evaporative Self-Assembly. *Angew. Chem., Int. Ed.* **2012**, *51*, 1534–1546.
12. Balakrishnan, K.; Datar, A.; Naddo, T.; Huang, J.; Oitker, R.; Yen, M.; Zhao, J.; Zang, L. Effect of Side-Chain Substituents on Self-Assembly of Perylene Diimide Molecules: Morphology Control. *J. Am. Chem. Soc.* **2006**, *128*, 7390–7398.
13. Tang, M. L.; Reichardt, A. D.; Miyaki, N.; Stoltenberg, R. M.; Bao, Z. Ambipolar, High Performance, Acene-Based Organic Thin Film Transistors. *J. Am. Chem. Soc.* **2008**, *130*, 6064–6065.
14. Palmer, L. C.; Stupp, S. I. Molecular Self-Assembly into One-Dimensional Nanostructures. *Acc. Chem. Res.* **2008**, *41*, 1674–1684.
15. Hoeben, F. J.; Jonkheijm, P.; Meijer, E.; Schenning, A. P. About Supramolecular Assemblies of π-Conjugated Systems. *Chem. Rev.* **2005**, *105*, 1491–1546.
16. Shimizu, T.; Masuda, M.; Minamikawa, H. Supramolecular Nanotube Architectures Based on Amphiphilic Molecules. *Chem. Rev.* **2005**, *105*, 1401–1444.
17. Li, D.; Huang, J.; Kaner, R. B. Polyaniline Nanofibers: A Unique Polymer Nanostructure for Versatile Applications. *Acc. Chem. Res.* **2008**, *42*, 135–145.
18. Martin, K. E.; Wang, Z.; Busani, T.; Garcia, R. M.; Chen, Z.; Jiang, Y.; Song, Y.; Jacobsen, J. L.; Vu, T. T.; Schore, N. E. Donor−Acceptor Biomorphs from the Ionic Self-Assembly of Porphyrins. *J. Am. Chem. Soc.* **2010**, *132*, 8194–8201.
19. Medforth, C. J.; Wang, Z.; Martin, K. E.; Song, Y.; Jacobsen, J. L.; Shelnutt, J. A. Self-Assembled Porphyrin Nanostructures. *Chem. Commun.* **2009**, 7261–7277.
20. Tian, Y.; Busani, T.; Uyeda, G. H.; Martin, K. E.; van Swol, F.; Medforth, C. J.; Montaño, G. A.; Shelnutt, J. A. Hierarchical Cooperative Binary Ionic Porphyrin Nanocomposites. *Chem. Commun.* **2012**, *48*, 4863–4865.
21. Bai, F.; Sun, Z.; Wu, H.; Haddad, R. E.; Coker, E. N.; Huang, J. Y.; Rodriguez, M. A.; Fan, H. Porous One-Dimensional Nanostructures through Confined Cooperative Self-Assembly. *Nano Lett.* **2011**, *11*, 5196–5200.
22. Bai, F.; Wu, H.; Haddad, R. E.; Sun, Z.; Schmitt, S. K.; Skocypec, V. R.; Fan, H. Monodisperse Porous Nanodiscs with Fluorescent and Crystalline Wall Structure. *Chem. Commun.* **2010**, *46*, 4941–4943.
23. Chen, W.; Peng, Q.; Li, Y. AlQ3 Nanorods: Promising Building Blocks for Optical Devices. *Adv. Mater.* **2008**, *20*, 2747–2750.
24. Fan, H.; Yang, K.; Boye, D. M.; Sigmon, T.; Malloy, K. J.; Xu, H.; López, G. P.; Brinker, C. J. Self-Assembly of Ordered, Robust, Three-Dimensional Gold Nanocrystal/Silica Arrays. *Science* **2004**, *304*, 567–571.
25. Fan, H.; Leve, E.; Gabaldon, J.; Wright, A.; Haddad, R. E.; Brinker, C. J. Ordered Two-and Three-Dimensional Arrays Self-Assembled from Water-Soluble Nanocrystal-Micelles. *Adv. Mater.* **2005**, *17*, 2587–2590.
26. Bai, F.; Wang, D.; Huo, Z.; Chen, W.; Liu, L.; Liang, X.; Chen, C.; Wang, X.; Peng, Q.; Li, Y. A Versatile Bottom-up Assembly Approach to Colloidal Spheres from Nanocrystals. *Angew. Chem., Int. Ed.* **2007**, *46*, 6650–6653.
27. Jo, H. J.; Jung, S. H.; Kim, H.-J. Synthesis and Hydrogen-Bonded Supramolecular Assembly of Trans-Dihydroxotin (IV) Tetrapyridylporphyrin Complexes. *Bull. Korean Chem. Soc.* **2004**, *25*, 1869–1873.
28. Kim, H.-J.; Jo, H. J.; Kim, J.; Kim, S.-Y.; Kim, D.; Kim, K. Supramolecular Self-Assembly of Tin (IV) Porphyrin Channels Stabilizing Single-File Chains of Water Molecules. *Cryst. Eng. Commun.* **2005**, *7*, 417–420.
29. Lee, S. J.; Hupp, J. T.; Nguyen, S. T. Growth of Narrowly Dispersed Porphyrin Namowires and Their Hierarchical Assembly into Macroscopic Columns. *J. Am. Chem. Soc.* **2008**, *130*, 9632–9633.
30. Zhang, X.; Dong, C.; Zapien, J. A.; Ismathullakhan, S.; Kang, Z.; Jie, J.; Zhang, X.; Chang, J. C.; Lee, C. S.; Lee, S. T. Polyhedral Organic Microcrystals: From Cubes to Rhombic Dodecahedra. *Angew. Chem., Int. Ed.* **2009**, *48*, 9121–9123.
31. Blankenship, R. *Molecular Mechanisms of Photosynthesis*; Blackwell: Oxford, 2002.
32. Mauzerall, D. C. Evolution of Porphyrins. *Clin. Dermatol.* **1998**, *16*, 195–201.
33. Bai, F.; Sun, Z.; Wu, H.; Haddad, R. E.; Xiao, X.; Fan, H. Templated Photocatalytic Synthesis of Well-Defined Platinum Hollow Nanostructures with Enhanced Catalytic Performance for Methanol Oxidation. *Nano Lett.* **2011**, *11*, 3759–3762.
34. Wang, Z.; Ho, K. J.; Medforth, C. J.; Shelnutt, J. A. Porphyrin Nanofiber Bundles from Phase-Transfer Ionic Self-Assembly and Their Photocatalytic Self-Metallization. *Adv. Mater.* **2006**, *18*, 2557–2560.
35. Guo, P.; Chen, P.; Ma, W.; Liu, M. Morphology-Dependent Supramolecular Photocatalytic Performance of Porphyrin Nanoassemblies: From Molecule to Artificial Supramolecular Nanoantenna. *J. Mater. Chem.* **2012**, *22*, 20243–20249.